



This is a repository copy of *A region segmentation method to measure multiple features using a tactile scanning probe*.

White Rose Research Online URL for this paper:  
<https://eprints.whiterose.ac.uk/145117/>

Version: Accepted Version

---

**Article:**

Li, F. [orcid.org/0000-0002-6413-3617](https://orcid.org/0000-0002-6413-3617), Hiley, J., Syed, T.M. et al. (2 more authors) (2019) A region segmentation method to measure multiple features using a tactile scanning probe. *International Journal of Computer Integrated Manufacturing*, 32 (6). pp. 569-579. ISSN 0951-192X

<https://doi.org/10.1080/0951192x.2019.1599431>

---

This is an Accepted Manuscript of an article published by Taylor & Francis in *International Journal of Computer Integrated Manufacturing* on 05/04/2019, available online:  
<http://www.tandfonline.com/10.1080/0951192X.2019.1599431>

**Reuse**

Items deposited in White Rose Research Online are protected by copyright, with all rights reserved unless indicated otherwise. They may be downloaded and/or printed for private study, or other acts as permitted by national copyright laws. The publisher or other rights holders may allow further reproduction and re-use of the full text version. This is indicated by the licence information on the White Rose Research Online record for the item.

**Takedown**

If you consider content in White Rose Research Online to be in breach of UK law, please notify us by emailing [eprints@whiterose.ac.uk](mailto:eprints@whiterose.ac.uk) including the URL of the record and the reason for the withdrawal request.



[eprints@whiterose.ac.uk](mailto:eprints@whiterose.ac.uk)  
<https://eprints.whiterose.ac.uk/>

# **A Region Segmentation Method to Measure Multiple Features Using a Tactile Scanning Probe**

Feng Li, Joseph Hiley, Tauseef Syed, Carl Hitchens, Miguel Garcia Lopez-Astilleros

Nuclear AMRC, University of Sheffield, Advanced Manufacturing Park,

Brunel Way, Rotherham, S60 5WG, United Kingdom

## **Abstract:**

Coordinate measuring machines have been widely used in industry to precisely measure parts for inspection or quality control. These machines use tactile or optical probes and a mechanism that can locate the position of the probe relative to surfaces and features of a workpiece. One of the main barriers to using a touch-trigger probe is the cumbersome programming work required to identify the probing points and for scan path planning. In this paper, we propose a practical data-segmentation method to continuously measure multiple features of the workpiece using a scanning probe. This approach takes advantage of fast data-capture capability of the scanning probe and, subsequently, the point dataset is segmented using the information extracted from the CAD model of the part. This methodology does not require tedious programming and all desired measurement results can be obtained from a single scan. The principle of the method is presented and the feasibility of the method is experimentally verified on a bridge-type Hexagon DEA Global CMM equipped with a Leitz LSP-X1 probe. The proposed method avoids manual operation errors and generates more sampling points than traditional methods; therefore, theoretically providing lower measurement uncertainty. The test results also indicate that the new method using a scanning probe is easy to implement and can save more than 90% measurement time in comparison with a conventional touch-trigger method.

Keywords: CMM; measurement; touch-trigger probe; scanning probe

## **1. Introduction**

One of the most difficult challenges during manufacturing-system development is to achieve total dimensional control of parts produced, creating statistical data analyses and part-to-part control. This may be achieved using various measurement instruments. Coordinate measuring machines (CMMs) are a common choice and have been widely used in the manufacturing industry for accurate, fast and reliable dimensional measurement of parts.

A CMM is a measuring system with the means to move a probing system and capability of determining the spatial coordinates of points on the surface of a workpiece. In a CMM system, the probe sensor is one of the most important elements and is crucial for the overall accuracy of a measurement result (Weckenmann, Estler et al. 2004). The most common probes for dimensional measurements are tactile and optical probing sensors, depending on whether the probes contact the surfaces of a workpiece. In addition, multi-sensor approaches have also been developed for coordinate metrology and the digitization of the surfaces of workpieces (Weckenmann, Jiang et al. 2009, Lu and Wang 2015). The major focus of this paper is on exploring the application of tactile probing systems for coordinate measurements. The working principal of tactile probes is based on a mechanical interaction with the workpiece and they usually measure in more than one direction.

Tactile probes are divided into two types: touch-trigger probes (TTPs), which contact the surface of the workpiece at discrete points, and scanning probes (SPs), which are in continuous contact with the

surface of the workpiece. TTPs, or discrete point probes, are the most popular probing system used on CMMs. TTPs use a discrete point probing method to record a set of points from the surface of the workpiece. In discrete point probing mode, the CMM lifts the probe head from the surface of the part, moves it forward a specified distance, then lowers it until the probe is once again in contact with the surface. This happens for every data point that is collected. TTPs are ideal for discrete point measurement but this single-point procedure is relatively slow. TTPs are unsuited for the efficient measurement of complex shaped workpieces, as well as applications in which large sets of point data are required, such as in form evaluation.

On the other hand, SPs send an uninterrupted flow of data back to the computer in response to the continuous deflection of the stylus. Data is gathered during movement when the stylus tip is placed in contact with the component to be measured and then is moved along the surface of the workpiece. They do not need the auxiliary movements required by TTPs. SPs often use two types of continuous scanning methods, open loop and closed loop, depending on whether the geometry of the workpiece is defined or undefined respectively. SPs have a much higher data acquisition rate: they can capture several hundred points per second in comparison to TTPs, which can usually gather 1-2 points per second. This advantage makes SPs suitable for measuring parts that consist of complex surfaces or measuring tasks that need a large number of points. SPs maintain contact with the workpiece and provide much more information about the form of a feature, which enables a better surface covering of the feature than TTPs (Álvarez, Cuesta et al. 2010). Therefore, form deviation measurement is another advantage of the SPs. In addition, SPs can also be used to acquire discrete points in a similar way to TTPs. Table 1 shows a comparison of the characteristics of both TTPs and SPs.

A CMM can be used to measure many different types of features, and the measurement uncertainty associated with each measurand may be quite different (Calvo, D'Amato et al. 2016, Calvo, D'Amato et al. 2016, Valdez and Morse 2017). The measuring/sampling strategy, for example, the selection of the number and position of points, can heavily influence the measured results (Choi, Kurfess et al. 1998, Jackman and Park 1998). Thoughtful path planning and careful selection of the location of probing points are essential when preparing an inspection program for a measurement task. The BS 7172:1989 (BS 1989) states that the distribution of measured data points should be designed to provide a uniform coverage of the workpiece, which will help to ensure that the points provide a genuine representation of the geometric feature. However, these operations mainly depend on the CMM operator's experience in the present state of the art. As an internationally-recognized guide, the Guide to the Expression of Uncertainty in Measurement (GUM) (BIPM, IFCC et al. 2008) suggests that the number of measurements should be large enough to ensure that the estimate of the measurand is reliable. According to the BS 7172:1989 (BS 1989), increasing the total number of points can be expected to have a statistically beneficial effect. This point is particularly important if the error of measurement is comparable to the machining error. The uncertainty associated with measurements with fewer points tends to be larger than the uncertainty associated with measurements with more points, with the return diminishing as the number of points is increased. At a certain point it is not worth collecting more data because the reduction in measurement uncertainty for a given increase in sample size is insignificant. By the same token, the more data points are collected the greater the cost associated with data collection. At some point it is no longer cost-effective to increase the sample size (Jiang and Chiu 2002). Thus, uncertainty reduction involves a cost-benefit analysis. For geometric feature dimensional measurement, it has been shown that ten times the number of parameters of a feature is a sufficient number of measurement points using a tactile probe, considering its measurement uncertainty according to literature (Kurfess and Banks 1995). However, in practice far fewer sampling points are usually taken considering the programming burden and measurement time.

Generally TTPs are a lot easier to program as compared to SPs, which require more complicated measurement routines. This means that one of the main disadvantages of SPs is that they usually need more programming effort to measure specific features than TTPs do; however, SPs can also measure discrete points and work as TTPs, and have much higher data capture rates. This does provide a possibility to enhance the measurement capability and flexibility of SPs by using a data segmentation and extraction method.

In this paper, a segmentation method is presented to process scanned point data to improve measurement efficiency and accuracy, taking advantage of the high data-output capability of SPs. Section 2 presents two methods to measure multiple geometric features using a trefoil artefact as an example: the traditional manual method using a TTP and the new automatic approach using a SP. Section 3 introduces the data segmentation and extraction methodologies. The best-fit algorithms used in this paper are described in Section 4. The experiment results using both methods are reported in Section 5. Finally, Section 6 summarises the key findings of this study and identifies topics for further investigation.

## 2. Methodologies

Before commencing measurement, preparations for the selected workpiece need to be considered, for example choice of probing styli, the measurement speed and measurement strategies.

The most commonly used styli in CMMs are ruby spheres. The choice of styli should depend on the specific scanning applications. The stylus tip diameter should be selected to be as large as possible to reduce the effects of surface finish. The stylus should be as short as possible to prevent excessive bending, but long enough to prevent risk of collision. The measuring speed (also known as speed of approach) is another factor that will affect the measurement results. In TTP mode, it has been observed that measurement errors are large but consistent at very slow measurement speed, due to the amount of time required by the slow speed to trigger the probe. At fast measurement speed, the probe triggers in a relatively short time and the deflection of the stylus is also significantly reduced (Flack 2001). However, with fast measurement speed larger forces are produced on contact and these contacts cause vibration and inertia effects, which may have a greater influence on the measurement results. Therefore, a compromise must be made between slow speeds, which may result in an unreasonably long time being required to complete the measurements, and fast speeds that may result in large impact forces on surface contact and reduced precision and accuracy of measurement. The effect of measuring speed for a specific machine can be ascertained through performance testing of the CMM e.g. measuring a standard artefact using different speeds, or the optimal measurement speed may be recommended by CMM manufactures.

In this section, a conventional method for performing measurement tasks using a TTP and a new strategy using a SP is presented. A trefoil artefact (see Fig.1 (a)), which includes multiple features to measure, has been selected as an example to illustrate how these methodologies work. The 3D CAD and 2D drawing of the part are shown in Fig. 1 (b) & (c), respectively. The dimensions of the artefact are 150 mm×150 mm×25 mm. Inspecting such a workpiece is a challenging task due to its relatively-complex geometry and multiple features. In each trefoil hole the features that need to be measured include: the angle  $\theta_A$  between segments  $A_1$  and  $A_2$  (the same naming convention is used to define angles  $\theta_B$  &  $\theta_C$  accordingly); the radii  $R_A$ ,  $R_B$  and  $R_C$  of arcs  $A$ ,  $B$  and  $C$ , respectively; the radius  $r$  of the maximum inscribed circle  $C$ , which is defined by segments  $L_1$ ,  $L_2$  and  $L_3$ . Fig. 1 (d) illustrates how the features are defined for measurement.

The conventional and proposed methods are as follows.

#### 1) Manual method using TTP mode

The conventional method is discrete-point probing each feature using a manual joystick or CAD model of the artefact (see Fig. 2. (a)), then performing a least-squares fit of the measurements. The main limitations of this method include: 1) tedious programming operations as probing locations must be carefully selected and multiple features need to be measured; 2) limited probing points can be taken because some features are relatively small, e.g. segment  $L_1$  as shown in Fig. 1. (d); 3) additionally, probing mistakes are easy to make because of the unclear boundaries between different features; for example, there are no clear boundary feature points on the artefact (see Fig. 1. (a)); if the probed points do not belong to the particular feature this will greatly affect the measuring results.

#### 2) Automatic method using SP mode

A new method that uses segmentation is proposed to measure multiple features. A SP is used to scan the full profile the trefoil hole (see Fig. 2. (b)) and the scanned points are processed to obtain the measured dimensions of different features. The detailed segmentation method is presented in Section 3 and the fitting algorithms are introduced in Section 4. The pros of this method are: 1) one scanning profile to obtain all features; 2) more sample points can be obtained to improve measurement accuracy; 3) there is no need to probe single feature; therefore, saving considerable CMM programming time; 4) this method can avoid manual probing mistakes and improve measurement reliability, especially when the CAD for the part is not available; 5) No need to analyse individual features using CMM software.

### 3. Data segmentation

The measured output from a SP is usually an open or closed loop of continuous point data, which can represent multiple geometric features. These point datasets need to be segmented/partitioned into patches and each patch can be fitted into a single, mathematically analysable shape. Segmentation involves grouping points from the original dataset into subsets, each of which logically belong to a single primitive feature. Segmentation is a crucial step towards the interpretation of 3D measurement data, especially point clouds measured using optical sensors e.g. laser or fringe projection techniques. Primitive type recognition and primitive fitting are key issues for computer aided manufacturing and assembly, geometric inspection etc. (Li, Longstaff et al. 2014, Aivaliotis, Michalos et al. 2018). Considerable research activities in shape segmentation have been explored in recent years. The methods for segmenting 3D data in engineering applications can be generally classified into three types: edge-based (Huang and Menq 2001, Demarsin, Vanderstraeten et al. 2007), region-growing (Besl and Jain 1988, Rabbani, van Den Heuvel et al. 2006) and hybrid-based (Woo, Kang et al. 2002, Liu and Xiong 2008, Le and Duan 2017). Chen and Liu (Chen and Liu 1997) presented a method for segmentation of free-form surfaces. The measurement point cloud is collected through a CMM and sliced by parallel planes. On each slicing plane, measured points are fitted by a 2D NURBS (Non-Uniform Rational B-Splines) spline. And then maximum curvature points on each NURBS spline can be calculated and marked as the boundary points. The point clouds can be segmented by these boundary points. In general, these techniques are developed to deal with continuous shape/surface segmentation problems. The shape information can be exploited to deal with segmentation problem. However, in our examples, or most cases using a CMM for dimensional measurement of geometric features, the point data is only taken from the specific features and dispersed. Therefore the above methods are not suitable for solving our data segmentation issues.

In this work, the data points captured using a tactile probe are segmented by defining the regions which can contain different features, by using the segmentation points (blue dots in Fig. 1. (c) & Fig. 3. (a)). These segmentation points can be read from the 2D drawing of the artefact and their coordinates are extracted at the same time. Because the relative positional relationships between the segmentation points and centre point of each hole (blue point in the centre - please see in Fig. 3. (a)) are fixed, all regions can be automatically calculated and defined using this relationship. The measured points falling into a specific region will be extracted for the least squares best fit of various geometric elements. Taking into account machining errors, the size of the segmentation region (0.5mm per side) is reduced to make sure the points in the region can accurately represent their corresponding geometric elements, as shown in Fig. 3. (a).

A Matlab toolbox is developed to read the 2D drawings and segment the data points which are measured from CMM. The script reads and the coordinates of entities in the .dxf file and saves the results as workspace variables. Then the regions to measure are highlighted and measurement results can be calculated using the algorithms which are introduced in Section 4.

#### 4. Least-squares best-fit geometric elements

After the segmentation process, the original point set is divided into subsets that can represent different geometric elements. These geometric features can be fitted using least-squares algorithms (Shakarji 1998). The various geometries that are used in this paper are 2D lines, radii of arcs and the maximum inscribed circle in the triangle. A measurement plane has been defined and all the 3D points have been projected into this specified plane e.g. xy-plane to calculate the feature values, which are described in Section 2.

##### 4.1. Least-squares best-fit line in a specified plane

A line in a plane can be specified by a point  $(x_o, y_o)$  on the line and the direction cosines  $(a, b)$  of the line.

$$a(x - x_o) + b(y - y_o) = 0 \quad (1)$$

$x_o$ ,  $y_o$ ,  $a$  and  $b$  are the desired parameters.

##### 4.2. Least-squares best-fit circle in a specified plane

A circle in the plane is specified by its centre  $(x_o, y_o)$  and radius  $r$ . Any point  $(x_i, y_i)$  on the circle satisfies the equation

$$(x - x_o)^2 + (y - y_o)^2 = r^2 \quad (2)$$

Equation (2) can be simplified as

$$x^2 + y^2 - ax - ay + \rho = 0 \quad (3)$$

where  $a = 2x_o$ ,  $b = 2y_o$  and  $\rho = x_o^2 + y_o^2 - r^2$ .

$a$ ,  $b$  and  $\rho$  are the desired parameters.

### 4.3. Maximum inscribed circle in the triangle

A triangle can be built using segments  $L_1$ ,  $L_2$  and  $L_3$ , and then the coordinates of three vertices can be calculated. The intersection point can be obtained from these two angle bisectors if two angle bisectors through any two vertices are made. Then this intersection point is the centre of the maximum inscribed circle in the triangle. The perpendicular distance from the centre to any side of the triangle is the radius of the maximum inscribed circle.

The above algorithms are integrated into the Matlab tool box, which directly generates measurement results using the point clouds after segmentation.

## 5. Experiments and results

The CMMs used in these experiments were a Hexagon Metrology DEA Global Silver (see Fig. 4 (a)) with maximum permissible error of length measurement ( $E_{L,MPE} = (3.0+3 \times L/1000) \mu\text{m}$  ( $L$  in mm)) and a Leitz PMM-C 12.10.7 CMM (Fig. 4 (b)) with  $E_{L,MPE} = (0.5+L/700) \mu\text{m}$  ( $L$  in mm), at a level of confidence greater than 99%, according to ISO 10360-1(ISO 2001), ISO 10360-2 (ISO 2009) and ISO 10360-4 (ISO 2000). In this paper, the term 'DEA' is used to represent the first CMM and 'PMM-C' is used to stand for the latter machine, respectively.

To test the measurement accuracy of DEA, a calibrated micrometre metric setting ring (Fig. 4 (c)) which is manufactured by Bowers Metrology, was selected as a reference artefact to verify the accuracy of TTP and SP used in this paper. The inner diameter of the setting ring is  $34.998 \text{ mm} \pm 0.0010 \text{ mm}$  at a level of confidence of approximately 95%. The uncertainty evaluation has been carried out in accordance with UKAS requirements. In addition, an arm assembly (maximum length 232 mm and depth 12 mm, please see Fig. 4 (d)) which is taken from RENISHAW QC20-W lathe calibration adaptor kit, has also been selected to further verify the accuracy of the proposed methods.

Both the equipment and artefacts have been soaked in a temperature-controlled metrology room for at least 24 hours before measurement, with the environmental temperature controlled at  $20 \pm 0.5 \text{ }^\circ\text{C}$ .

Several terms used to describe the different meaning of speed are explained:

- Move Speed: The speed of the stylus/probe when not approaching the surface of part.
- Touch Speed: The speed of the stylus when it is approaching the surface of workpiece and the probe is starting to collect discrete points in touch-trigger mode.
- Scan speed: The speed of the stylus when it is contacting and passing over the surface of the workpiece with a continuous movement in scanning mode.

During the tests, the move speed is set to 100 mm/s for both modes with a touch speed of 2 mm/s for TTP mode. These parameters are recommended by the CMM manufacturer. The manufacturer also advises that the scan speed should be less than 5 mm/s for the CMM used in this paper; however, a 5 mm/s scanning speed causes a discontinuous contact between the stylus tip of probe and the surface, according to our experiments. Therefore the scan speed of 1 mm/s and 2 mm/s for SP mode are used to measure the trefoil artefact, separately.

Next, the accuracy of the DEA TTP and SP was tested, and then the results of the two measurement methods were compared using the trefoil artefact.

### **5.1. Accuracy tests using DEA TTP & SP**

The probe used in this experiment is a three-axis Leitz LSP-X1 probe that can conduct touch trigger and scanning measurements in a single probe system and is able to execute touch-trigger probing and scanning. Table 2 presents the specifications of the LSP-X1.

In this test, 4, 11 and 30 points are selected uniformly on the internal circumference of the setting ring, when performing the accuracy test for the TTP mode. A circle in a specified plane can be defined by three parameters (Equation 2), therefore 30 probed points should be sufficient for the measurement of this feature using a contact probe according to reference (Kurfess and Banks 1995). The number of points for scanning mode is set to 202 because of the high data capture rate of the SP and the scan speed is set to 2 mm/s. The process was repeated five times and the measured diameter of the setting ring and standard deviation of measurement results are presented in Table 3.

Table 3 shows that all the results are very close to the calibrated value of the setting ring. The standard deviations also demonstrate that the measurement results are robust. Both TTP and SP can provide accurate measurement results and the number of probing points does not affect the measurement results, if the artefact possesses a very small form error.

### **5.2. Measurement results from different methods using DEA**

The top three trefoil holes (see Fig. 1. (a)) are used to illustrate the proposed method. All profiles of holes are measured with a depth of 10 mm from the top surface.

The measured points are aligned to the nominal model of the artefact using the best-fit method. In this paper, the nominal data is fixed and the measured data is transformed. The method introduced in literature (Li, Stoddart et al. 2017) is exploited to find the optimum rigid transformation. After alignment, the probed point data is processed using the proposed method. The data segmentation and fitting results are shown in Fig. 5. (a) and (b), respectively.

In this case, four methodologies are used to test their accuracy: the conventional manual method using TTP with low density (TTP-L) and high density (TTP-H) points; the proposed automatic method using SP with slow (1 mm/s, SP-S) and faster scan speed (2 mm/s, SP-H). The number of probing points and measurement time for each single trefoil hole using different methods are shown in Table 4.

Table 4 indicates that, in comparison with the TTP methods, the SP method requires much less measurement time but can capture many more data points. The artefact used in this paper is only a small sample piece from a steam-generator baffle-support plate. The original part may contain thousands of these trefoil holes; therefore our method can save considerable measurement time, which means this approach has a significant advantage in industrial applications.

The deviations of the measured results from nominal value using DEA TTP and SP are listed in Table 5 & 6, separately.

From Table 5 and 6, significant deviations have been observed between the measurement results using low density points (TTP-L) and other three methods (TTP-H, SP-S and SP-F methods), which have exceeded the maximum permissible error of DEA CMM used in this paper. In general, the consistency of results measured using high density points (TTP-H, SP-S and SP-F methods) are satisfactory. The Pearson's correlation coefficient between different methods are also computed and listed in Table 7.

Table 7 summarises that the Pearson's correlation coefficients between results measured from high density points are very close to 1, which further validates our above conclusions. A comparison of points measured using low density points (measured from TTP-L method) and high density points (measured from TTP-H, SP-S and SP-F methods) are displayed in Fig. 6 (a) and (b), respectively.

According to statistical rules, a much higher number of data points must be taken to ensure the measurement accuracy, especially in the presence of unknown form error (Hocken, Raja et al. 1993). However, this increase in sampling points is directly related to CMM programming difficulties and measurement time when using a conventional discrete point probing method. The proposed method using a SP can capture a significantly higher number of points within a shorter time, and can therefore theoretically provide better accuracy when compared to the method commonly used with a TTP.

### ***5.3. Accuracy tests using different CMMs***

To further verify the accuracy of the proposed methods, an arm assembly has been selected to use as an artefact for comparative measurements using the different CMMs and inspection methods. This workpiece contains a relatively complex geometric features and therefore it is an ideal artefact to verify the methodologies.

A benchmark measurement of the dimension of the artefact was made using the Leitz PMM-C CMM, which has a better accuracy according to the machine specifications and relevant ISO standards. Then the values measured using the Leitz PMM-C CMM were compared with the results measured using the Hexagon DEA CMM and the proposed segmentation method.

The 3D CAD model is shown in Fig. 7. (a) and the features that need to be measured are illustrated in Fig. 7. (b).

The measuring depth was set to 5 mm from the top surface of the part to measure the radii  $R_a$  and  $R_b$ . Two lines of points with measuring depths of 5 mm and 8 mm respectively from the top surface of artefact, were probed to construct a plane. Another plane can be constructed using same measurement strategy and then the angle  $\theta$  was defined between these two planes. All three measurement methodologies follow the same measuring strategy. The measurements results are demonstrated in Table 8.

From Table 8, DEA SP results are slightly closer than DEA TTP method using the PMM-C results as reference. In general both measurement results are within the allowable tolerance according to the CMMs manufactures' specifications.

### ***5.4 Task specific uncertainties evaluation***

In this case, the measurement uncertainty mainly results from measurement equipment (CMM) and measurement environment (Wen, Zhu et al. 2012). The significant uncertainty contributions, which are suggested by literature (Barini, Tosello et al. 2010, ISO 2011), can be listed as follows:

#### **(1) Repeatability**

The repeatability study has been conducted according to (ISO 2000, ISO 2009) and the estimated standard uncertainty  $u_r$  can be calculated from series of repeated measurements. The  $u_r$  values for PMM-C, DEA-TTP and DEA-SP are 0.34, 0.84, 1.00  $\mu\text{m}$ , respectively.

#### **(2) Effect of dirt**

The uncertainty component  $u_d$  from the dirt is estimated as 0.1  $\mu\text{m}$  by referring to literature (Barini, Tosello et al. 2010).

### (3) Effect of temperature difference

The temperature difference between CMMs and the artefacts is observed to maximum 0.5  $^{\circ}\text{C}$  during the measurement process. The linear coefficient of thermal expansion is assumed to be 1.1  $\mu\text{m}/(100\text{mm} \times ^{\circ}\text{C})$  for CMM and the parts. The influence can be calculated:

$$\alpha_{td} = \Delta T \times \alpha \times H = 0.5\text{ }^{\circ}\text{C} \times 1.1 \frac{\mu\text{m}}{100\text{mm} \times ^{\circ}\text{C}} \times \sqrt{232^2 + 12^2} \text{mm} = 1.28 \mu\text{m}$$

The U-distribution is assumed and the uncertainty component  $u_{td}$  which is introduced by temperature difference is (ISO 2011):

$$u_{td} = \frac{1.28}{\sqrt{2}} = 0.91 \mu\text{m}$$

### (4) Effect of thermal expansion

The observed maximum deviation from standard reference temperature (20  $^{\circ}\text{C}$ ) is 1  $^{\circ}\text{C}$ .  $\pm 1\text{ }^{\circ}\text{C}$  is assumed as there is no information about the sign of this deviation. The difference in thermal expansion coefficients (CMM and parts) is assumed to be less than 10% (ISO 2011). The influence is calculated:

$$\alpha_{te} = \Delta T \times \alpha \times H = 1\text{ }^{\circ}\text{C} \times 1.1 \frac{\mu\text{m}}{100\text{mm} \times ^{\circ}\text{C}} \times \sqrt{232^2 + 12^2} \text{mm} \times 10\% = 0.26 \mu\text{m}$$

A U-distribution is assumed and the uncertainty component  $u_{te}$  from the thermal expansion coefficient is (ISO 2011):

$$u_{te} = \frac{0.26}{\sqrt{2}} = 0.18 \mu\text{m}$$

### (5) Drift and hysteresis of CMMs

The uncertainty component  $u_h$  from the drift and hysteresis of CMM is estimated as 0.2  $\mu\text{m}$  according to (ISO 2011).

As all above uncertainty contributions are considered as uncorrelated, the combined standard uncertainty of different methods can be calculated by the formula (BIPM, IFCC et al. 2008):

$$u_0 = \sqrt{u_r^2 + u_d^2 + u_{td}^2 + u_{te}^2 + u_h^2} \quad (4)$$

The combined standard uncertainty and expanded standard uncertainty (95.45% measurement confidence,  $k=2$ ) are listed in Table 9.

## 5.5. Discussion

In this section, a setting ring is used to test the accuracy of DEA TTP & SP and then a trefoil artefact is selected to illustrate the viability of our presented technique in an industrial application. In addition, an arm assembly is also used to further verify the accuracy of our proposed method.

Overall, the following conclusions have been drawn:

- 1) When measuring an artefact which has been calibrated or has good form error, the number of measured points does not significantly affect the measurement accuracy. The minimum and recommend number of points for different geometric features can be found in (BS 1989).
- 2) When measuring a part with unknown form error, the number of measured points greatly influences the measurement results. Therefore ten times the number of parameters of feature for the measurement points is recommended, as concluded by the literature (Kurfess and Banks 1995).
- 3) There was no evidence that the scan speed (1 mm/s and 2 mm/s in this paper) significantly affects the measuring results when using a SP. However, a relatively slow scanning speed (1 mm/s in this case) will be recommended, especially when measuring features with tight tolerances.
- 4) The test results using a trefoil artefact indicate that the new method using a SP is easy to implement, and can reduce the measurement time by more than 90% comparison with the conventional TTP method, when measuring a part with unknown form error. The data segmentation technique can also be expanded to measure other open and closed loop or continuous multiple geometric features, for example quatrefoil shape and gear measurement etc.
- 5) The accuracy of the new methodologies using the DEA SP is further verified using a more accurate PMM-C CMM. The conventional method using the DEA TTP is also compared with the PMM-C CMM. The measurement results indicate the new method using SP is still superior to TTP method in terms of accuracy but overall both methods obtain satisfied results. The task specific uncertainties using different methods have also evaluated. The uncertainty evaluation results indicate the DEA TTP (2 mm/s touch speed) and DEA SP (2 mm/s scanning speed) have similar measurement accuracy but the SP method is ideal for measurement applications where dense point clouds data are needed and time budget is limited.

## 6. Conclusions and future work

The use of conventional TTPs for CMM has become a common choice in dimensional metrology. However, some barriers still need to be addressed, specifically the time required to programme measurement routines, low number of sampling points due to limited programming and measuring time and the selection of sampling points because of the probing difficulties. This scenario greatly reduces measurement efficiency and reliability of the measurement results. This work shows the feasibility of a SP, with increased data acquisition rate, to be used for the continuous multi-feature measurements. The scanned point dataset is processed by the proposed data segmentation method and all the measurement results can be calculated using least square best-fit algorithms. In theory, the proposed method using a SP can avoid manual sample point position errors and generate many more sampling points, which can provide improved measurement accuracy compared with the traditional TTP approach. Scanning probing is therefore ideal for measurement applications where the form of a feature is a significant element of the overall error budget, or where complex surfaces need to be inspected. In addition, our methodology does not need complex sampling strategy and path planning, which can save considerable programming time. The test results using a trefoil artefact indicate that the proposed method using a SP can reduce the measurement time by more than 90% comparison with the conventional TTP method.

As the inspection of large machined components (those being over 2 metre) is a costly and difficult activity, on-machine inspection has the potential to reduce time, cost and risk associated with the

manufacture of large-volume components. The logistics involved in relocating large components from the machining centre to a CMM are difficult and often account for a significant amount of the overall manufacturing time. Further work will involve the evaluation of the performance of probing systems on a multiple axis large scale machining centres. A measurement system analysis (MSA) will be carried out to qualify measurement systems for the use on machine centres by quantifying accuracy, precision and stability. Then the region segmentation method described in this paper will be replicated using a SP installed on a CNC machining centre. The measured results will be compared with the CMM results detailed in this study. Results of this research this will greatly expand the knowledge base pertaining to on-machine inspection.

## Acknowledgment

The authors gratefully acknowledge the support of the High Value Manufacturing (HVM) Catapult and thank Robert Elgar and Kevin S Monaghan for the assistance with CMM measurements.

## References

- Aivaliotis, P., G. Michalos and S. Makris (2018). "Cooperating robots for fixtureless assembly: modelling and simulation of tool exchange process." International Journal of Computer Integrated Manufacturing **31**(12): 1235-1246.
- Álvarez, B., E. Cuesta, S. Martínez, J. Barreiro and P. Fernández (2010). Implementation of decision rules for CMM sampling in a KBE system. Proceedings of the 36th international MATADOR conference, Springer.
- Barini, E. M., G. Tosello and L. De Chiffre (2010). "Uncertainty analysis of point-by-point sampling complex surfaces using touch probe CMMs: DOE for complex surfaces verification with CMM." Precision Engineering **34**(1): 16-21.
- Besl, P. J. and R. C. Jain (1988). "Segmentation through variable-order surface fitting." IEEE Transactions on Aerospace and Electronic Systems **10**(2): 167-192.
- BIPM, I., I. IFCC, I. IUPAC and O. ISO (2008). Evaluation of measurement data—guide for the expression of uncertainty in measurement. JCGM 100: 2008.
- BS (1989). "BS, 7172:1989." Guide to Assessment of position, size and departure from nominal form of geometric features.
- Calvo, R., R. D'Amato, E. Gómez and R. Domingo (2016). "Integration of Error Compensation of Coordinate Measuring Machines into Feature Measurement: Part I—Model Development." Sensors **16**(10): 1610.
- Calvo, R., R. D'Amato, E. Gómez and R. Domingo (2016). "Integration of Error Compensation of Coordinate Measuring Machines into Feature Measurement: Part II—Experimental Implementation." Sensors **16**(10): 1705.
- Chen, Y. H. and C. Y. Liu (1997). "Robust segmentation of CMM data based on NURBS." The International Journal of Advanced Manufacturing Technology **13**(8): 530-534.
- Choi, W., T. R. Kurfess and J. Cagan (1998). "Sampling uncertainty in coordinate measurement data analysis." Precision Engineering **22**(3): 153-163.
- Demarsin, K., D. Vanderstraeten, T. Volodine and D. Roose (2007). "Detection of closed sharp edges in point clouds using normal estimation and graph theory." Computer-Aided Design **39**(4): 276-283.
- Flack, D. (2001). "Measurement Good Practice Guide No. 43: CMM Probing." National Physical Laboratory, London, UK.
- Hocken, R. J., J. Raja and U. Babu (1993). "Sampling issues in coordinate metrology." Manufacturing Review **6**: 282-282.
- Huang, J. and C.-H. Menq (2001). "Automatic data segmentation for geometric feature extraction from unorganized 3-D coordinate points." IEEE Transactions on Aerospace and Electronic Systems **17**(3): 268-279.

ISO, B. E. (2011). "BS EN ISO 14253-2:2011." Geometrical product specifications (GPS) - Inspection by measurement of workpieces and measuring equipment. Part 2: Guidance for the estimation of uncertainty in GPS measurement, in calibration of measuring equipment and in product verification.

ISO, E. (2000). "EN ISO, 10360-4:2000." Geometrical Product Specification (GPS), Acceptance and reverification tests for coordinate measuring machines (CMM) Part 4: CMMs used in scanning measuring mode.

ISO, E. (2001). "EN ISO, 10360-1:2001." Geometrical Product Specifications (GPS), Acceptance and Reverification Tests for Coordinate Measuring Machines (CMM) Part 1: Vocabulary.

ISO, E. (2009). "EN ISO, 10360-2:2009." Geometrical Product Specifications (GPS), Acceptance and Reverification Tests for Coordinate Measuring Machines (CMM) Part 2: CMMs used for measuring linear dimensions.

Jackman, J. and D.-K. Park (1998). "Probe orientation for coordinate measuring machine systems using design models." Robotics and Computer-Integrated Manufacturing **14**(3): 229-236.

Jiang, B. C. and S.-D. Chiu (2002). "Form tolerance-based measurement points determination with CMM." Journal of Intelligent Manufacturing **13**(2): 101-108.

Kurfess, T. R. and D. L. Banks (1995). "Statistical verification of conformance to geometric tolerance." Computer-Aided Design **27**(5): 353-361.

Le, T. and Y. Duan (2017). "A primitive-based 3D segmentation algorithm for mechanical CAD models." Computer Aided Geometric Design.

Li, F., A. P. Longstaff, S. Fletcher and A. Myers (2014). "Rapid and accurate reverse engineering of geometry based on a multi-sensor system." The International Journal of Advanced Manufacturing Technology **74**: 369-382.

Li, F., D. Stoddart and C. Hitchens (2017). "Method to automatically register scattered point clouds based on principal pose estimation." Optical Engineering **56**(4): 044107-044107.

Liu, Y. and Y. Xiong (2008). "Automatic segmentation of unorganized noisy point clouds based on the Gaussian map." Computer-Aided Design **40**(5): 576-594.

Lu, K. and W. Wang (2015). "A multi-sensor approach for rapid and precise digitization of free-form surface in reverse engineering." International Journal of Advanced Manufacturing Technology **79**.

Rabbani, T., F. van Den Heuvel and G. Vosselmann (2006). "Segmentation of point clouds using smoothness constraint." International Archives of Photogrammetry, Remote Sensing and Spatial Information Sciences **36**(5): 248-253.

Shakarji, C. M. (1998). "Least-squares fitting algorithms of the NIST algorithm testing system." Journal of Research-National Institute of Standards and Technology **103**: 633-641.

Valdez, M. O. and E. P. Morse (2017). "The role of extrinsic factors in industrial task-specific uncertainty." Precision Engineering.

Weckenmann, A., T. Estler, G. Peggs and D. McMurtry (2004). "Probing Systems in Dimensional Metrology." CIRP Annals - Manufacturing Technology **53**(2): 657-684.

Weckenmann, A., X. Jiang, K. D. Sommer, U. Neuschaefer-Rube, J. Seewig, L. Shaw and T. Estler (2009). "Multisensor data fusion in dimensional metrology." CIRP Annals - Manufacturing Technology **58**(2): 701-721.

Wen, X.-L., X.-C. Zhu, Y.-B. Zhao, D.-X. Wang and F.-L. Wang (2012). "Flatness error evaluation and verification based on new generation geometrical product specification (GPS)." Precision Engineering **36**(1): 70-76.

Woo, H., E. Kang, S. Wang and K. H. Lee (2002). "A new segmentation method for point cloud data." International Journal of Machine Tools and Manufacture **42**(2): 167-178.

Table 1 The comparison of TTP & SP

|                 | TTP  | SP  |
|-----------------|--|---|
| Measuring speed | 1-2 points/sec   | Up to several thousand points/sec   |
| Advantages      | 1. Cost effective<br>2. Compact and rugged<br>3. Low stylus wear           | 1. Higher data capture rates<br>2. Suitable for applications that require many data points  |
| Disadvantages   | 1. Low data capture speed<br>2. Sparse density of the acquired points data | 1. Relatively high costs<br>2. May need more complicated routines to measure specific feature<br>3. Not suitable for materials that are easily scratched. |
| Applications    | 1. Size and position of the feature<br>2. Parts have stable form accuracy  | 1. Complex surfaces<br>2. Form deviation evaluation   |

Table 2 Specifications of the Leitz LSP-X1 scanning probe system

| Technical figure   | Parameter                | Value                        |
|--|--------------------------|------------------------------|
|  | Dimensions               | Ø 30 × 109 mm                |
|  | Weight                   | 100 g                        |
|  | Resolution               | < 0.1 µm                     |
|  | Measuring range          | ± 2 mm in all axes           |
|  | Linear stiffness         | 1.2 N/mm                     |
|  | Stylus joint             | M3                           |
|  | Max. stylus weight       | 20 g (incl. stylus clamping) |
|  | Max. Stylus length range | Up to 115 mm                 |

Table 3 Setting ring measurement results using DEA

| Unit: mm        | 1      | 2      | 3      | 4      | 5      | Std. Dev. |
|-----------------|--------|--------|--------|--------|--------|-----------|
| TTP (4 points)  | 35.000 | 35.000 | 34.999 | 35.000 | 35.000 | 0.0001    |
| TTP (11 points) | 35.000 | 35.000 | 34.999 | 35.000 | 35.000 | 0.0001    |
| TTP (30 points) | 34.999 | 34.999 | 34.999 | 34.999 | 34.999 | 0.0000    |
| SP (202 points) | 35.000 | 35.000 | 35.000 | 35.000 | 35.000 | 0.0000    |

Table 4 Number of points & measurement time for trefoil artefact using DEA

|                  | TTP-L | TTP-H | SP-S | SP-F |
|------------------|-------|-------|------|------|
| Number of points | 57    | 392   | 392  | 392  |
| Time (s)         | 159   | 1050  | 81   | 42   |

Table 5 Deviations of measurements results using DEA-TTP

| Results of deviations | Hole 1 |        | Hole 2 |        | Hole 3 |        |
|-----------------------|--------|--------|--------|--------|--------|--------|
|                       | TTP-L  | TTP-H  | TTP-L  | TTP-H  | TTP-L  | TTP-H  |
| $\theta_A$ (°)        | 0.105  | -0.050 | 0.086  | -0.039 | 0.103  | -0.026 |
| $\theta_B$ (°)        | 0.166  | 0.092  | 0.088  | 0.057  | 0.114  | 0.077  |
| $\theta_C$ (°)        | 0.139  | 0.109  | 0.111  | 0.119  | 0.184  | 0.152  |
| $R_A$ (mm)            | -0.240 | -0.145 | -0.149 | -0.164 | -0.195 | -0.159 |

|                     |        |        |        |        |        |        |
|---------------------|--------|--------|--------|--------|--------|--------|
| R <sub>B</sub> (mm) | 0.005  | -0.109 | -0.104 | -0.105 | -0.032 | -0.109 |
| R <sub>C</sub> (mm) | -0.330 | -0.217 | -0.273 | -0.170 | -0.215 | -0.166 |
| r (mm)              | -0.028 | -0.026 | -0.028 | -0.027 | -0.029 | -0.028 |

Table 6 Deviations of measurements results using DEA-SP

| Results of deviations | Hole 1 |        | Hole 2 |        | Hole 3 |        |
|-----------------------|--------|--------|--------|--------|--------|--------|
|                       | SP-S   | SP-F   | SP-S   | SP-F   | SP-S   | SP-F   |
| θ <sub>A</sub> (°)    | -0.053 | -0.055 | -0.039 | -0.036 | -0.025 | -0.024 |
| θ <sub>B</sub> (°)    | 0.092  | 0.081  | 0.058  | 0.055  | 0.076  | 0.072  |
| θ <sub>C</sub> (°)    | 0.106  | 0.098  | 0.117  | 0.115  | 0.153  | 0.156  |
| R <sub>A</sub> (mm)   | -0.148 | -0.133 | -0.170 | -0.161 | -0.162 | -0.147 |
| R <sub>B</sub> (mm)   | -0.109 | -0.119 | -0.108 | -0.104 | -0.110 | -0.111 |
| R <sub>C</sub> (mm)   | -0.218 | -0.211 | -0.172 | -0.171 | -0.171 | -0.183 |
| r (mm)                | -0.026 | -0.026 | -0.027 | -0.027 | -0.028 | -0.028 |

Table 7 Pearson correlation coefficient of results using DEA

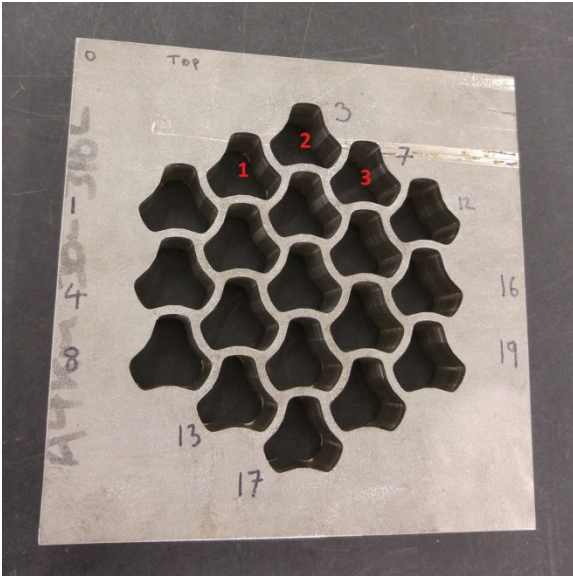
|               | Hole 1 | Hole 2 | Hole 3 | Average |
|---------------|--------|--------|--------|---------|
| TTP-L & TTP-H | 0.8892 | 0.8979 | 0.9264 | 0.9045  |
| TTP-L & SP-S  | 0.8897 | 0.8987 | 0.9298 | 0.9061  |
| TTP-L & SP-F  | 0.8695 | 0.9054 | 0.9276 | 0.9008  |
| TTP-H & SP-S  | 0.9999 | 0.9998 | 0.9999 | 0.9999  |
| TTP-H & SP-F  | 0.9986 | 0.9998 | 0.9974 | 0.9986  |
| SP-S & SP-F   | 0.9982 | 0.9997 | 0.9978 | 0.9986  |

Table 8 Deviations of measurements results using different CMMs

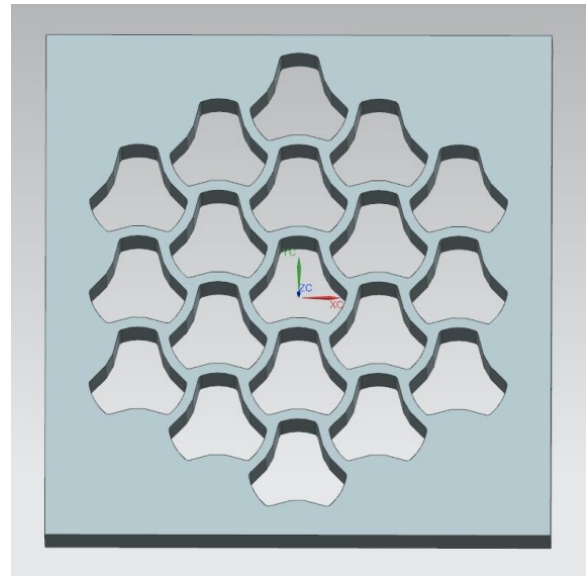
| Results of measurements | PMM-C  | DEA-TTP | DEA-SP |
|-------------------------|--------|---------|--------|
| R <sub>a</sub> (mm)     | 14.012 | 14.015  | 14.015 |
| R <sub>b</sub> (mm)     | 14.008 | 14.010  | 14.009 |
| θ (°)                   | 44.793 | 44.798  | 44.791 |

Table 9 Combined standard uncertainty & expanded standard uncertainty

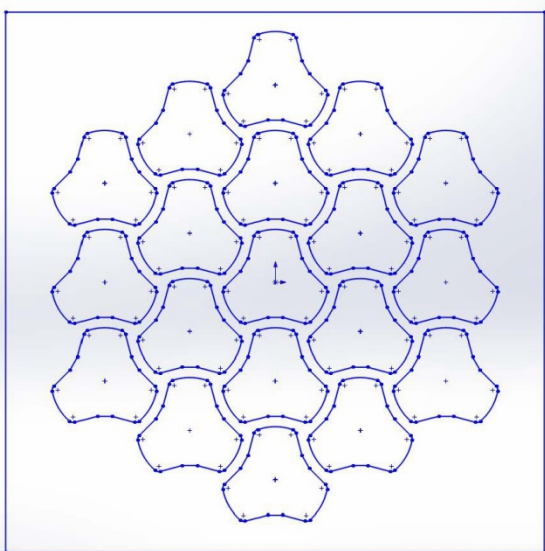
| Unit: μm                 | PMM-C | DEA-TTP | DEA-SP |
|--------------------------|-------|---------|--------|
| Combined STD uncertainty | 1.01  | 1.27    | 1.38   |
| Expanded STD uncertainty | 2.02  | 2.55    | 2.76   |



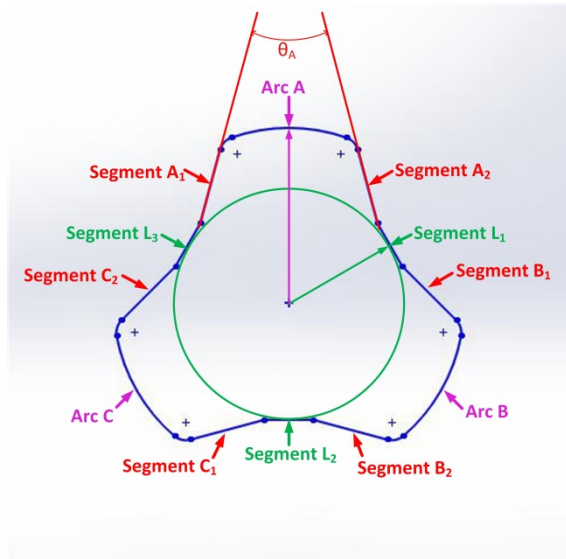
(a) Trefoil artefact



(b) 3D CAD model of the artefact

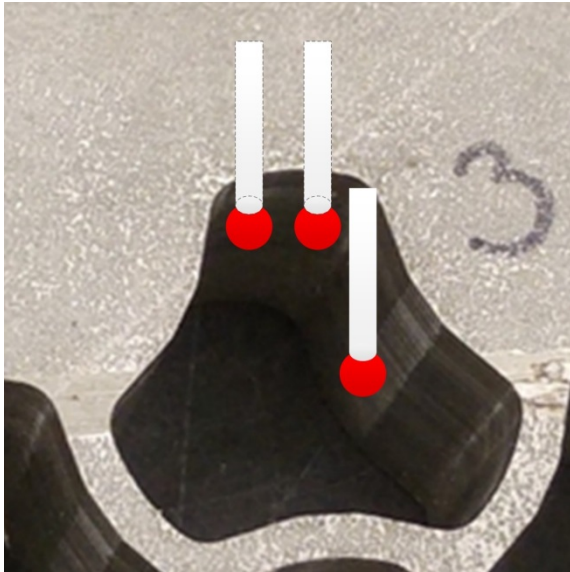


(c) 2D drawing of top surface of the artefact

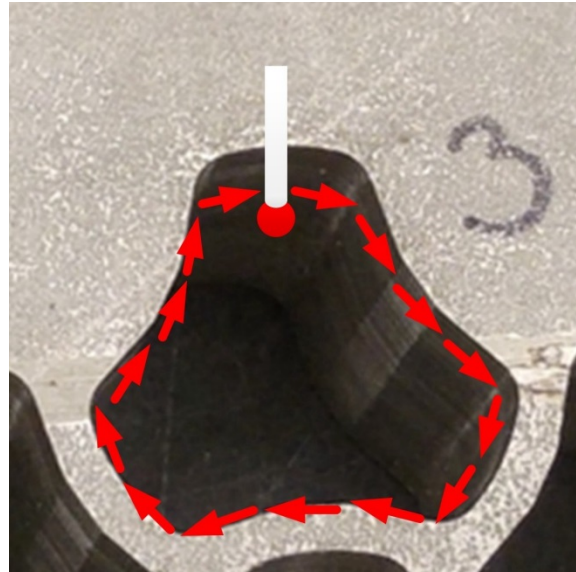


(d) Features to measure

Fig. 1. Artefact to measure

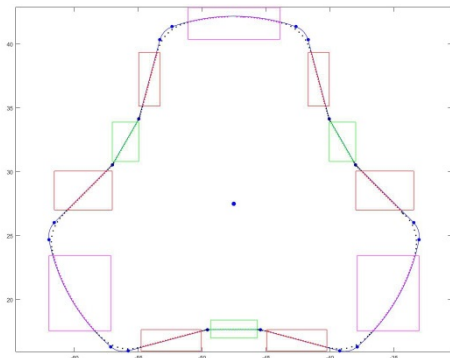


(a) Manual touch-trigger method

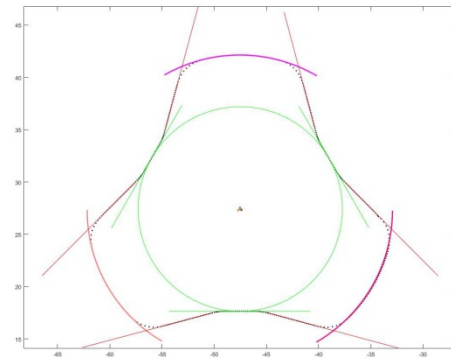


(b) Automatic scanning method

Fig. 2. Measurement strategies



(a) Defining segmentation regions



(b) Least squares best fit geometric elements

Fig. 3. Data segmentation and fitting



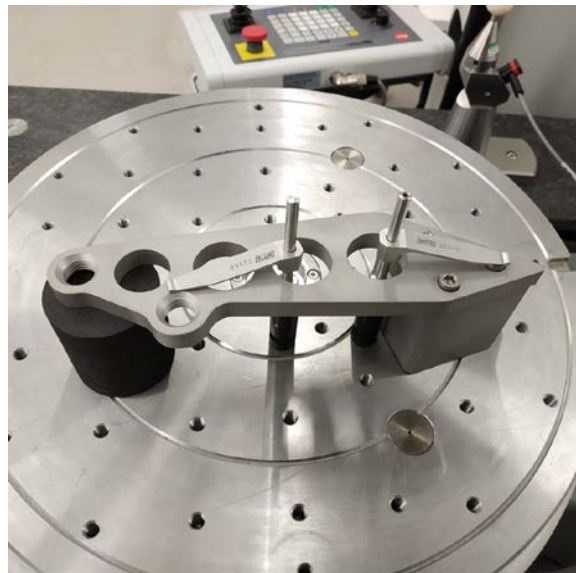
(a) Hexagon DEA Global Silver CMM



(b) Leitz PMM-C 12.10.7 CMM

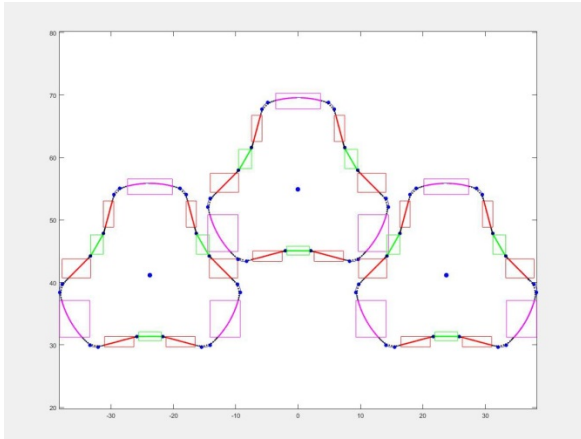


(c) Micrometre metric setting ring

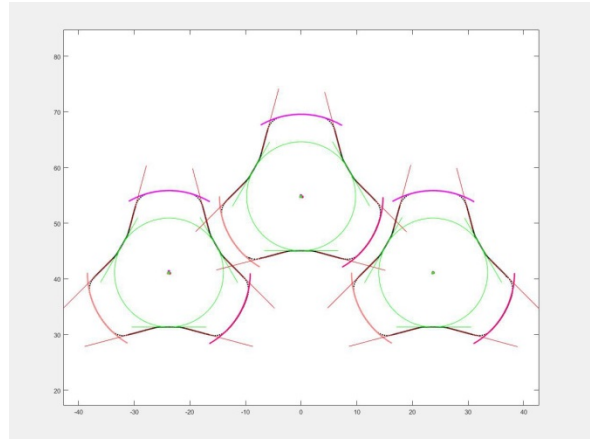


(d) RENISHAW QC20-W arm assembly

Fig. 4. Elements of the test

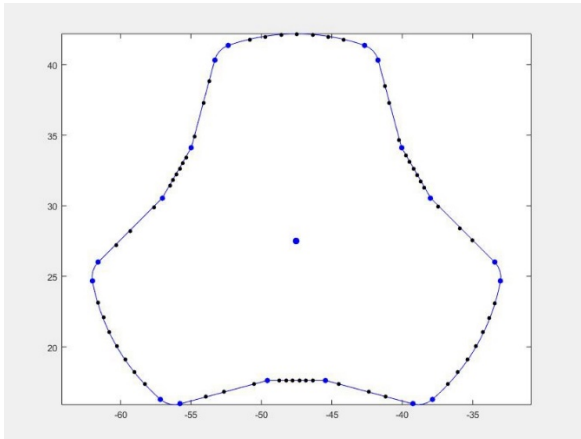


(a) Data segmentation

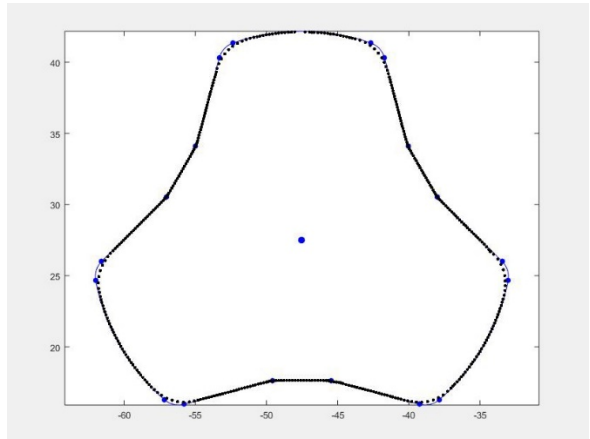


(b) Least squares best fit results

Fig. 5. Data segmentation and best fitting

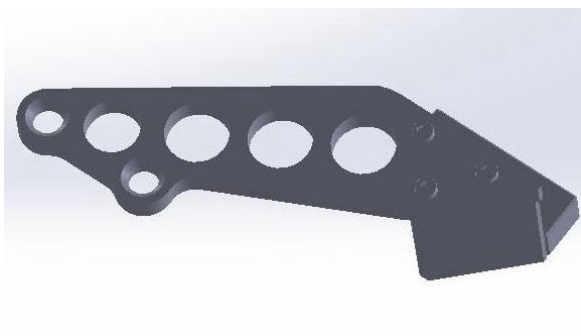


(a) Low density points

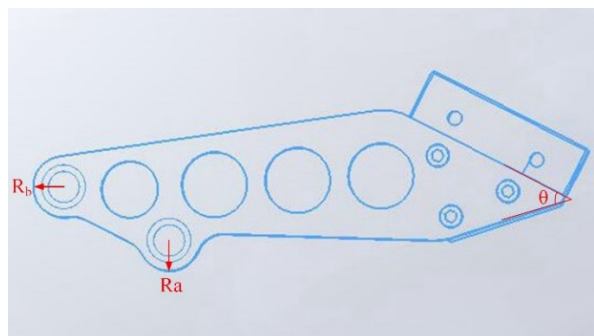


(b) High density points

Fig. 6. Data points (black) measured using different methods



(a) 3D CAD model of the arm assembly



(b) Features to measure

Fig. 7. CAD models of the QC20-W arm assembly